ELSEVIER

Image and Vision Computing 19 (2000) 25–31

image AND vision COMPUTING

www.elsevier.com/locate/imavis

Reconstructing a 3D structure from serial histological sections

S. Ourselin*, A. Roche, G. Subsol, X. Pennec, N. Ayache

INRIA Sophia Antipolis, Epidaure Project, 2004 Route des Lucioles BP 93, 06902 Sophia Antipolis Cedex, France

Received 30 August 1999; revised 14 April 2000; accepted 27 June 2000

Abstract

We consider the problem of aligning histological sections for 3D reconstruction and analysis. The method we propose is based on a block-matching strategy that allows us to compute local displacements between the sections. We then collect these local measures to estimate a rigid transformation. Our emphasis is on the necessity to use a robust approach for this estimation step. The process is integrated within a multi-scale scheme to improve both accuracy and computation time. We prove experimentally that we can reach sub-pixel accuracy and we show some results of aligning histological sections from a rat's brain and a rhesus monkey's brain.

Keywords: Histological sections; 3D reconstruction; Registration; Robust estimation; Block matching

1. Introduction

1.1. Presentation of the problem

Histological sections provide useful information for the diagnosis or the study of a pathology. To obtain histological sections, the anatomical structure is first fixed using paraffin embedding or by cryogenization. Then it is trimmed into thin sections with a constant inter-section gap. The microscopic images are then scanned using a digital camera. Very often, the acquisition is performed independently for each section and the alignment is lost as we can see in Fig. 1. Hence, in order to perform a 3D reconstruction of the anatomical structure, we need to register the sections to recover the original alignment.

The 3D reconstruction from serial sections may lead to numerous applications at both the microscopic and the macroscopic levels. At the microscopic level, which corresponds to a magnification greater than 100, the 3D reconstruction study allows one to define new and more accurate histological and cytological parameters, such as the tumoral angiogenis in oncology, the fibrosis development in hepatitis, the cellular distortions in prion diseases and, more generally, to quantify many physiological and pathological phenomena. At the macroscopic level, the 3D reconstruction study allows one to study objects that are too small to be accurately dissected and too large to be analyzed based only on the 2D slices.

With average quality data, which can be obtained in current laboratories, different problems can arise. When laying the sample on the cover-glass, some spots can appear and the edges of the cover-glass can be within the field of view of the camera (as in the example of Fig. 1). All this can create many artifacts in the background. The intensity contrast can be different from one slice to another (e.g. due to staining), and changes in the lighting can occur during the digitalization. Moreover, during sectioning, the edges of the sections can be distorted or even torn and, more generally, the whole section can be deformed. Nevertheless, we will assume in the following that the distortions remain small enough to consider the transformation between two consecutive sections as being rigid.

Different methods have been proposed in the literature to align histological sections. The most common one is the manual registration using interactive operator alignment [6,15,26]. It is a non-reproducible method because it is user-dependent and it could depend on the structure the user wants to focus on. Moreover, it is a tremendous task and it cannot be used when the number of sections is large.

Other methods are based on fiducial markers. Useful markers can be obtained by sticking needles in the structure before cutting [9]. Nevertheless, the resulting tracks may be unreliable if the cutting planes are not perfectly orthogonal to the needles. Moreover, creating such tracks can destroy a part of the structure and then impede any post-mortem diagnosis.

* Corresponding author. Tel.: +33-492-387159; fax: +33-492-387669.
E-mail address: sebastien.ourselin@sophia.inria.fr (S. Ourselin).

0262-8856/01/$ - see front matter
PII: S0262-8856(00)00052-4

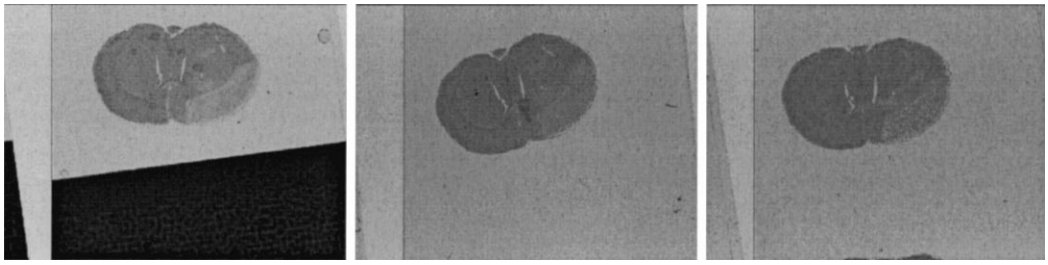

Fig. 1. Three consecutive stained rat's brain histological sections. We can see how they are misaligned.

Features automatically extracted from the images have also been used to drive registration. A classical method consists of segmenting the anatomical structure in two successive sections, and then computing the principal-axes transformation (PAT) [1,10]. Schormann and Zilles argue in Ref. [28] that the precision of this method remains very limited. Much-improved results are obtained by matching contours [4,34], edges [12,13], or points [23].

Finally, intensity-based methods were also proposed in the context of section registration. These methods search for the transformation that maximizes a measure of the similarity in intensity between corresponding pixels. Some authors have used the correlation coefficient as a similarity measure [2,10], while others have used mutual information [14].

To our knowledge, there is no quantitative comparison between these approaches. This would be an interesting future work, although this is far beyond the scope of this article, in which we concentrate on a new, robust, intensity-based approach.

1.2. Motivation

A particular difficulty of section registration is that the structures represented in two successive slices are not perfectly equivalent from an anatomical point of view. Severe morphological differences may be observed if the inter-slice gap is large, as can be seen in Fig. 2.

Our method does not assume that two consecutive sections are anatomically equivalent. It only assumes local similarities and tries to find the rigid transformation that matches a maximum of similar regions. Local displacements between two sections are first computed using a block-matching strategy [11]. The rigid transformation is then estimated from these matches as the solution of a robust regression problem. Robustness is a key point because we want the transformation to be governed by the majority of matches instead of being averaged over all the displacements. This process is iterated within a multi-scale scheme to deal with large displacements and to obtain accurate results.

We detail the different steps of the algorithm in Section 2. In Section 3, we analyze its accuracy and robustness quantitatively, with respect to the relative displacement of two sections. Section 4 presents the results of reconstructing a rat's brain and a Rhesus monkey's brain. Finally, we propose several research tracks for future work in Section 5.

2. Algorithm

The algorithm takes as input two section images: a reference image I_1 and a floating image I_2 with the same dimensions $X \times Y$. The output will be the transformation T and the image $I = I_2 \circ T^{-1}$, which is aligned with I_1. The whole process follows from a multi-scale iterative scheme where, at each stage, two successive tasks are performed. The first is computing a displacement field between I_1 and the current floating image I; this is done through a block-matching strategy. The second is gathering these displacements to estimate a rigid transformation S. Updating the current transformation according to $T \leftarrow S \circ T$, we get the new floating image I by resampling only once the image I_2 in terms of the new T. Then, the scheme parameters are modified and the process is iterated.

2.1. The block-matching step

Block-matching techniques, which were previously

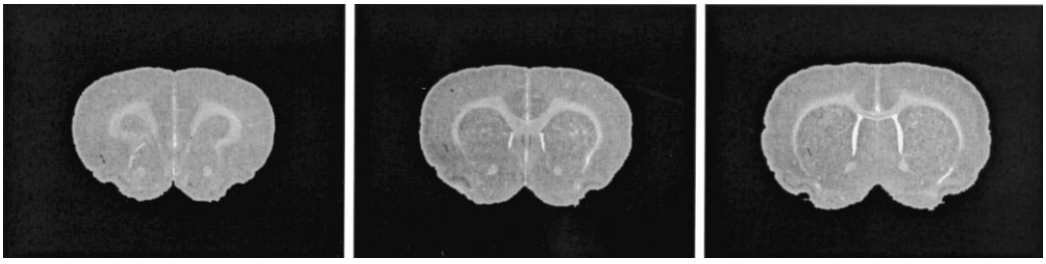

Fig. 2. Three consecutive sections from a rat's brain dataset as an illustration of morphological changes from one section to another. The inter-slice gap is 0.4 mm.

developed for video compression [11], have inspired several algorithms in image registration [5,8]. The basic principle is to move a block $\mathscr{B}'$ of the floating image in its neighborhood and to compare it to the blocks $\mathscr{B}$ that have similar positions in the reference image. The best corresponding block $\mathscr{B}$ allows one to define a vector between the centers of the blocks $\mathscr{B}$ and $\mathscr{B}'$.

The block-matching algorithm involves three parameters: the size N of the blocks (each block contains $N \times N$ pixels), the half-width Ω of the neighborhood which is searched, and the spacing Δ_1 between two consecutive blocks $\mathscr{B}'$ to be displaced. For each block $\mathscr{B}'$, $4\Omega^2$ neighboring blocks have to be tested, which may be computationally expensive. Hence, we generally sub-sample the authorized displacements of a block according to a step Δ_2. This results in the following algorithm, where the coordinates (i,j) of a block are taken as its left upper corner.

- For $(i = 0; i \leq X - N; i = i + \Delta_1)$
- For $(j = 0; j \leq Y - N; j = j + \Delta_1)$
- Consider the block $\mathscr{B}'_{ij}$ in image I:
  - For $(k = i - \Omega; k \leq i + \Omega; k = k + \Delta_2)$
  - For $(l = j - \Omega; l \leq j + \Omega; l = l + \Delta_2)$
  - Compute the value C_{ij}^{kl} of a given similarity measure between $\mathscr{B}'_{ij}$ and the block B_{kl} in I_1.
- Let $\mathscr{B}_{mn} = \arg\max C_{ij}^{kl}$ be the block that maximizes the similarity measure. It defines the displacement vector between $(i + N/2, j + N/2)$ and $(m + N/2, n + N/2)$.

One important feature of the block-matching process is the choice of the similarity measure. As discussed in Refs. [24,32], it should depend on the expected relationship between the intensities of corresponding pixels of two successive sections. In the case of histological sections, it is reasonable to assume that this relationship is affine within a block (locally affine). Hence, the similarity between two blocks can be measured using the correlation coefficient [3,22]:

$$C(\mathscr{B}_{ab}, \mathscr{B}'_{uv}) = \frac{1}{N^2} \sum_{i=0}^{N-1} \sum_{j=0}^{N-1} \left[\frac{1}{\sigma_I(a,b)\sigma_{I_1}(u,v)} \times [I(a+i, b+j) - \bar{\imath}_{(a,b)}][I_1(u+i, v+j) - \bar{\imath}_{1(u,v)}] \right] \quad (1)$$

where $\bar{\imath}_{(a,b)}$ and $\sigma_I(a,b)$ ($\bar{\imath}_{1(u,v)}$ and $\sigma_{I_1}(u,v)$) are the mean and standard deviation, respectively, of the block $\mathscr{B}_{ab}$ ($\mathscr{B}'_{uv}$).

In our block-matching experience, the main problem when using a similarity measure is that the blocks are not always comparable. This may occur due to morphological differences between the sections, background artifacts, or simply because the displaced block is almost uniform. This leads to a certain number of bad matches: in our experiments, typically 20% of the displacement vectors are due to outliers.

This problem can be partially alleviated by constraining the authorized displacements to privileged directions, as is classically done in optical flow formulations [8,31]. In doing so, however, we may remove too much information on the actual motion we want to measure. Instead, we propose to keep the displacement field as is and to estimate the global rigid transformation using a robust approach.

2.2. Computing a robust estimate of the rigid transformation

The block-matching step provides a list of corresponding 2D points, x_k and y_k. Assuming that there exists a rigid transformation between the sections, the problem is to estimate a two-by-two rotation matrix R and a translation vector $t = (t_1, t_2)$ that characterize the inter-section displacement. A standard approach to solving such a problem is to perform a least squares (LS) regression on the matched points:

$$(\hat{R}, \hat{t}) = \arg \min_{R,t} \sum_k \|r_k\|^2, \quad (2)$$

where $r_k = y_k - Rx_k - t$ are the residual errors and $\| \|$ denotes the Euclidean norm.

The main advantages of the LS estimator are that the solution is unique and is quickly computed. Several closed forms are discussed in Ref. [7]. However, LS is known to have poor robustness properties [25], in the sense that its solution is sensitive to outliers. In our experiments, the LS estimate is generally inaccurate.

A number of robust estimation techniques have been investigated in the literature of point matching [33], among which M-estimators appear to be the most straightforward alternative to LS. The M-estimators generalize LS by replacing the squared residuals $\|r_k\|^2$ in Eq. (2) with another function, yielding:

$$(\hat{R}, \hat{t}) = \arg \min_{R,t} \sum_k \rho(\|r_k\|), \quad (3)$$

where ρ is a symmetric, positive-valued function with a unique minimum at zero. The basic principle is to reduce the influence of outliers by choosing a slowly increasing ρ-function. One usually distinguishes between two classes of M-estimators depending on whether ρ is convex or not. Although M-estimators from the latter class tend to be less sensitive to large errors, the uniqueness of the solution is guaranteed only for convex ρ-functions [16].

In our particular case, we do not expect large errors since the y_k points as well as the x_k points have bounded norms. We have thus chosen a convex M-estimator, namely the L_1 estimator that corresponds to the simple function $\rho(x) = |x|$. Unlike in the LS estimation, only a numerical solution can be obtained. To do so, we use Powell's method [19], which does not manipulate the derivatives of the criterion to be minimized.

We note that other candidates such as the Huber or "Fair" estimators are theoretically more efficient than L_1 [25]. The main advantage of L_1 over those M-estimators is that it does not require estimating a scale parameter beforehand. After

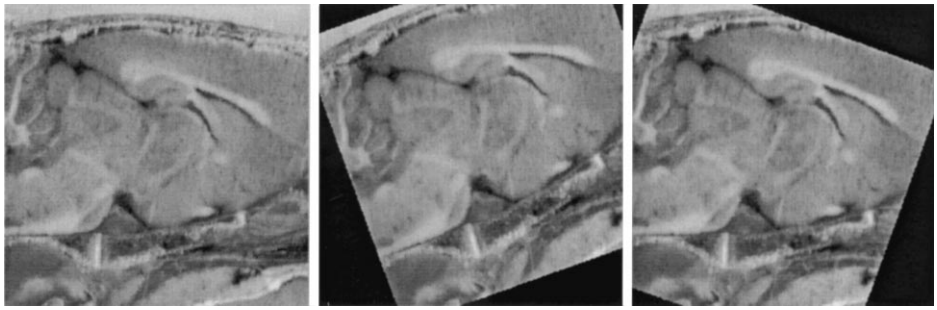

Fig. 3. Left and center: two consecutive slices shifted by a rotation of 20°. Right: the second slice is registered to the first one.

computing the L_1 estimate, however, we may compute such a scale parameter and refine the solution using another *M*-estimator. In practice, we did not observe significant improvement over the L_1 solution and thus we decided to suppress the refinement step.

Another observation is that our results were often slightly improved when replacing the Euclidean norm of the residuals in Eq. (3) with their 1-norm (or Manhattan distance), i.e. $\|r_k\|_1 = |r_{k1}| + |r_{k2}|$, where (r_{k1}, r_{k2}) are the components of r_k in the coordinate system of the reference section. This might sound surprising since choosing the 1-norm causes the solution to be dependent upon the particular coordinate system in which the points (x_k, y_k) are given. On the other hand, the block-matching algorithm is itself coordinate-dependent and, thus, there is no reason why the estimated transformation should not be so.

The implementation of this coordinate-wise L_1 estimator using Powell's method yields the same computation time as for the conventional L_1 estimator. This is actually the default estimation method that is used in our implementation.

2.3. Multi-scale implementation

To obtain a precise displacement field, we should choose low values for Δ_1 and Δ_2. On the other hand, the complexity of the block-matching process is proportional to $(N^2\Omega^2)/(\Delta_1^2\Delta_2^2)$ [20]. We propose a multi-resolution method to achieve a good trade-off between accuracy and complexity. We start at a coarse scale with large values for N, Ω, Δ_1, and Δ_2. We then progressively refine the scale by decreasing these parameters. In this manner, we find large but inaccurate displacements at the higher level, and smaller but more accurate ones as the scale decreases. The parameters of the algorithm are initialized according to the image size. Our usual choice is:

$$N = \min\left(\frac{X, Y}{8}\right), \quad \Omega = N, \quad \Delta_1 = \frac{N}{4}, \quad \Delta_2 = 4.$$

At each iteration, we compute a variation measure δ between the new transformation $S \circ T$ and the previous one, T. Let P_1–P_4 be the four corners of the floating image I_2:

$$\delta = \frac{1}{4}\sum_{i=1}^{4} \|S \circ T(P_i) - T(P_i)\|^2. \tag{4}$$

The decision rule for changing the scale is to compare δ to a given threshold ϵ. If $\delta > \epsilon$, we iterate at the same scale; otherwise, we iterate with each parameter halved. Notice that the complexity is then constant at each level. The whole process is stopped when the block size becomes

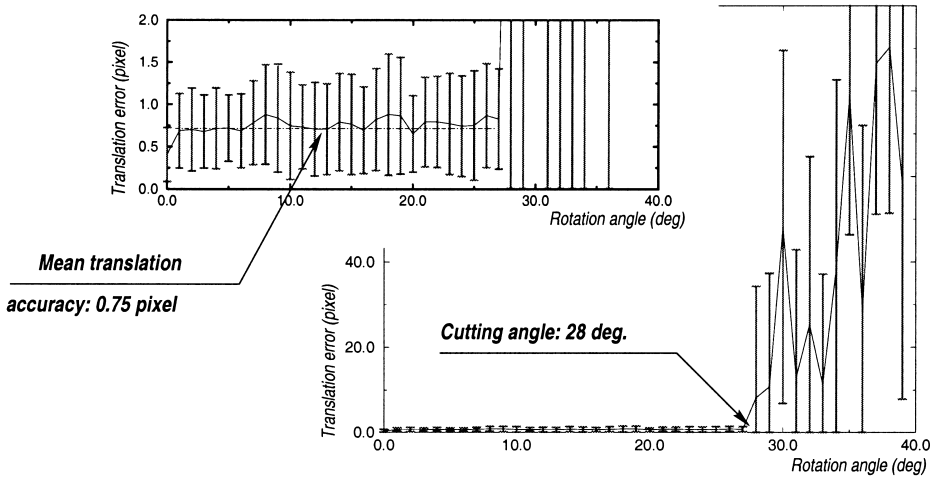

Fig. 4. Accuracy of the estimated translation with respect to the angle of rotation. The upper left window shows a magnified view of the graph.

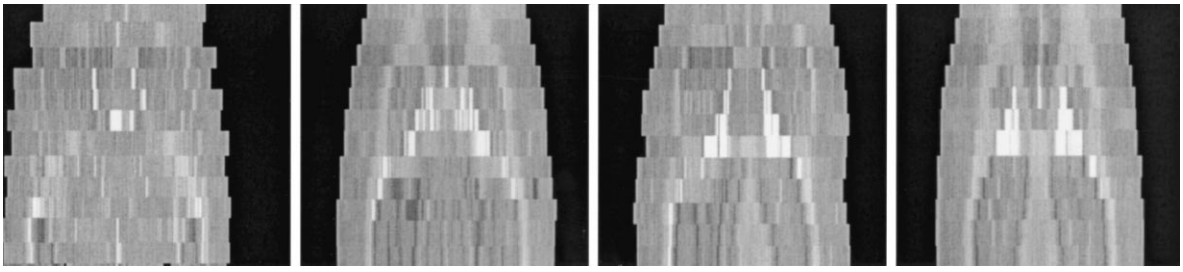

Fig. 5. Median perpendicular view of the section set. Left: initial data. Middle left: after registration using the principal axes method. Middle right: after registration using global correlation. Right: after registration using the presented method.

inferior to a given limit (typically, $N_{\text{lim}} = 4$), after which the information content of the blocks is considered no longer sufficient to draw meaningful comparisons.

3. Robustness and accuracy analysis

To characterize the performance and the robustness of the algorithm, we used the data of a rat brain from the UCLA rat brain atlas [29] where the cryoplaned block-face was consistently positioned during section acquisition. Thus, the "ground truth" registration is the identity. Then, we randomly resampled consecutive sections with a known rigid transformation (see Fig. 3) and we studied the error $\delta\theta = |\theta - \hat{\theta}|$ on the rotation angle and the error $\delta t = \|t - R_{\theta}\hat{t}\|$ on the translation component [21]. In the following, the experiments are performed on three couples of contiguous sections from the middle of the brain. To speed up the statistics (we performed more than 1600 registrations), we extracted a sub-image of size 256×256 in the 1024×1024 images.

3.1. Sensitivity to rotation

A first experiment with a translation smaller than 40 pixels shows that the algorithm is almost completely insensitive to this kind of translation. Thus, in the first step, we can focus on the parameter θ alone.

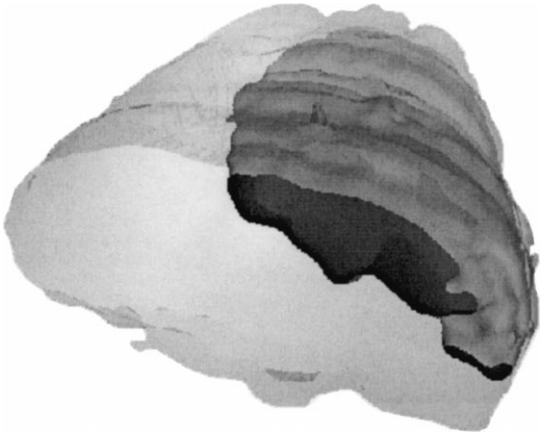

Fig. 6. Reconstruction with segmentation of an ischaemia area.

In Fig. 4, we show the translation error δt with respect to the rotation angle θ. Each point on the graph is the average value for 50 registrations with random translations. On the large scale graph, we clearly see that the algorithm always converges for rotations of an angle less than $\theta_{\text{cut}} = 28°$. For higher values, the algorithm occasionally diverges. On the small scale graph, we see that the accuracy of the translation is statistically constant (RMS of 0.75 pixels) when the algorithm converges. We observed exactly the same type of graphs for the error on the rotation angle, with the same cutting angle value and a mean accuracy of 0.2°.

3.2. Sensitivity to translation

We repeated the above experiment, but keeping rotations under 15° with a translation range from 0 to 100 pixels. We obtained very similar results: a statistically constant accuracy of the transformation for translations less than a cut-off value of $t_{\text{cut}} = 52$ pixels and sporadic to continual divergence above this threshold.

This cut-off value approximately corresponds to 1.5 times the half-width of the block neighborhood at the higher level ($\Omega = 32$ pixels). Since the block matching is optimized with a maximal displacement of $\sqrt{2}\Omega$, this means that at least 50% of the corresponding blocks need to be within the search area, which is in accordance with what we expected. Hence, the size of the convergence basin for translations is directly linked to the size of the block neighborhood Ω and can be extended by taking larger blocks.

4. Results

4.1. Rat's brain

We realigned several datasets from rat brains containing from 20 to 26 sections with a resolution of 768×576 pixels (0.03 mm × 0.085 mm) and an inter-section gap of 0.4 mm. This was achieved without any preprocessing step. The registration of two sections took around 1 min on a standard PC (OS Linux), 450 MHz, 256 MBytes of RAM. In Fig. 5, we compare the results of aligning the sections using the presented method with the PAT method, and with the maximization of the correlation coefficient over the whole image (using Powell's method as an optimization scheme). This

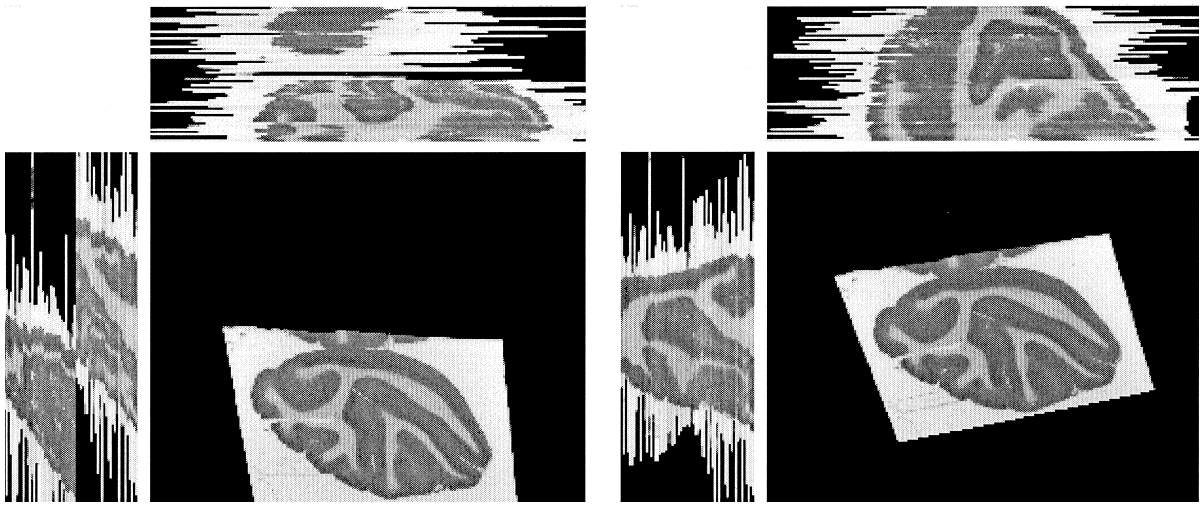

Fig. 7. Rhesus monkey's brain. Left: three orthogonal views of the initial section stack. Right: the same views after realignment.

dataset corresponds to the sections shown in Fig. 2. We notice that the inner structures are better observed in our result image.

In Fig. 6, we segmented the cortical surface and an ischaemia area from another reconstructed block using digital topology techniques. This data corresponds to the sections shown in Fig. 1.

4.2. Rhesus monkey's brain

We have realigned 170 sections from a rhesus monkey's brain [30]. These sections, with a resolution of 636×512 pixels ($0.085\ \text{mm} \times 0.085\ \text{mm}$) and an inter-section gap of 0.1 mm, correspond to the posterior third of the left hemisphere. The result is shown in Fig. 7 and compared to the original data. One may notice that large displacements have been recovered. Using the reconstructed volume, we segmented the cortical surface and the white matter by combining 3D digital topology techniques and deformable models [18] (see Fig. 8).

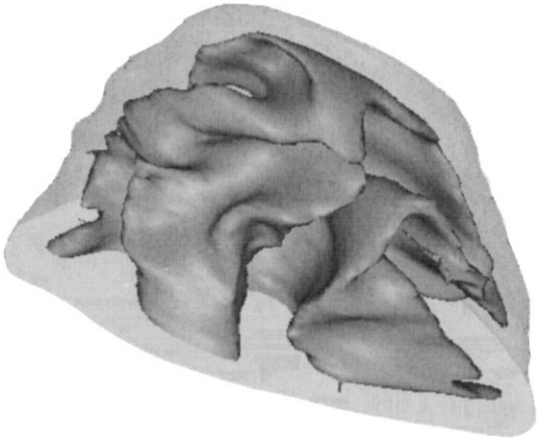

Fig. 8. 3D reconstruction of the rhesus monkey's brain with segmentation of the white matter.

5. Conclusions

We have presented a new method to align histological sections. It alternates between computing local displacements using a block-matching strategy and robustly estimating a rigid transformation from these matches. The whole process is integrated in a multi-scale scheme to improve the computation time as well as the registration accuracy. Our algorithm has been shown experimentally to provide subpixel accuracy while being able to compensate for large displacements.

An extension of the method to non-rigid registration would be useful to compensate for geometrical distortions that occur during sectioning. This is a difficult problem because part of the inter-section deformations are due to morphological differences and must *not* be corrected. Instead of evaluating geometrical distortions slice by slice, perhaps a better approach is to non-rigidly register the 3D reconstructed structure (after rigid realignment of the sections) with another 3D modality such as MR [27] or PET [17].

Another current limitation of the method is that the registrations are performed independently for each pair of contiguous sections. As a consequence, registration errors are integrated from the beginning of the stack to the end of the stack. When dealing with a large number of sections, this might prevent any reliable 3D reconstruction. Such error propagation might be reduced by placing spatial constraints on the reconstructed structure.

Acknowledgements

The authors would like to thank Elf and Sanofi-Research, Montpellier (France), Paul Thompson, LONI, UCLA (USA) for the rat's brain datasets and Wim Vanduffel, Katholieke Universiteit Leuven (Belgium), for the rhesus monkey's

brain dataset. We would also like to thank Dr Christophe Sattonnet for constant interaction and suggestions, and Janet Bertot for proofreading.

References

[1] N.M. Alpert, J.F. Bradshaw, D. Kennedy, J.A. Correia, The principal axes transformation — a method for image registration, J. Nucl. Med. 31 (10) (1990) 1717–1722.
[2] A. Andreasen, A.M. Drewes, J.E. Assentoft, N.E. Larsen, Computer-assisted alignment of standard serial sections without use of artificial landmarks. A practical approach to the utilization of incomplete information of 3-D reconstruction of the hippocample region, J. Neurosci. Meth. 45 (1992) 199–207.
[3] G.L. Brown, A survey of image registration techniques, ACM Comput. Surv. 24 (4) (1992) 325–376.
[4] F.S. Cohen, Z. Yang, Z. Huang, J. Nissanov, Automatic matching of homologous histological sections, IEEE Trans. Biomed. Engng 45 (5) (1998) 642–649.
[5] D.L. Collins, A.C. Evans, ANIMAL: validation and applications of nonlinear registration-based segmentation, Int. J. Pattern Recog. Artif. Intell. 8 (11) (1997) 1271–1294.
[6] M.H. Deverell, J.R. Salisbury, M.J. Cookson, J.G. Holman, E. Dykes, F. Whimster, Three-dimensional reconstruction: methods of improving image registration and interpretation, Anal. Cell. Pathol. 5 (1993) 253–263.
[7] D.W. Eggert, A. Lorusso, R.B. Fisher, Estimating 3D rigid body transformations: a comparison of four major algorithms, Special Issue on Performance Characteristics of Vision Algorithms, Mach. Vis. Appl. 9 (5/6) (1997) 272–290.
[8] T. Gaens, F. Maes, D. Vandermeulen, P. Suetens, Non-rigid multimodal image registration using mutual information, in: W.M. Wells, A. Colchester, S. Delp (Eds.), Proceedings MICCAI'98, Lecture Notes in Computer Science, vol. 1496, Springer, Berlin, 1998, pp. 1099–1106.
[9] A.F. Goldszal, O.J. Tretiak, P.J. Hand, S. Bhasin, D.L. McEachron, Three-dimensional reconstruction of activated columns from 2-[14C]deoxy-D-glucose data, Neuroimage 2 (1995) 9–20.
[10] L.S. Hibbard, R.A. Hawkings, Objective image alignment for three-dimensional reconstruction of digital autoradiograms, J. Neurosci. Meth. 26 (1988) 55–74.
[11] A.K. Jain, Image data compression: a review, Proc. IEEE 69 (3) (1981) 349–389.
[12] P.A. Kay, R.A. Robb, D.G. Bostwick, J.J. Camp, Robust 3-D reconstruction and analysis of microstructures from serial histologic sections, with emphasis on microvessels in prostate cancer, in: K.H. Höhne, R. Kikinis (Eds.), Visual. Biomed. Comput., Lecture Notes in Computer Science, vol. 1131, Springer, Berlin, 1996, pp. 129–134.
[13] B. Kim, K.A. Frey, S. Mukhopadhyay, B.D. Ross, C.R. Meyer, Co-registration of MRI and autoradiography of rat brain in three-dimensions following automatic reconstruction of 2D data set, in: N. Ayache (Ed.), Computer Vision, Virtual Reality and Robotics in Medicine, Lecture Notes in Computer Science, vol. 905, Springer, Berlin, 1995, pp. 262–266.
[14] B. Kim, J.L. Boes, K.A. Frey, C.R. Meyer, Mutual information for automated unwarping of rat brain autoradiographs, Neuroimage 5 (1997) 31–40.
[15] Visualization in Biomedical Microscopies: 3-D Imaging and Computer Applications, in: A. Kreite (Ed.), VCH, 1992.
[16] P. Meer, D. Mintz, D.Y. Kim, A. Rosenfeld, Robust regression methods in computer vision: a review, Int. J. Comput. Vis. 6 (1991) 59–70.
[17] M.S. Mega, S.S. Chen, P.M. Thompson, R.P. Woods, T.J. Karaca, A. Tiwari, H.V. Vinters, G.W. Small, A.W. Toga, Mapping histology to metabolism: coregistration of stained whole-brain sections to premortem PET in Alzheimer's disease, Neuroimage 5 (1997) 147–153.
[18] J. Montagnat, H. Delingette, Globally constrained deformable models for 3D object reconstruction, Signal Processing 71 (2) (1998) 173–186.
[19] W.H. Press, B.P. Flannery, S.A. Teukolsky, W.T. Vetterling, Numerical Recipes in C, Cambrige University Press, Cambridge, 1992.
[20] S. Ourselin, A. Roche, G. Subsol, X. Pennec, C. Sattonnet, Automatic alignment of histological eections for 3D reconstruction and analysis, Technical Report 3595, INRIA, December 1998 (electronic version: http://www.inria.fr/RRRT/RR-3595.html).
[21] X. Pennec, J.P. Thirion, A framework for uncertainty and validation of 3D registration methods based on points and frames, Int. J. Comput. Vis. 25 (3) (1997) 203–229 (electronic version: http://www.inria.fr/RRRT/RR-2470.html).
[22] G.P. Penney, J.W. Weese, J.A. Little, P. Desmedt, D.L.G. Hill, D.J. Hawkes, A comparison of similarity measures for use in 2D–3D medical image registration, First International Conference on Medical Image Computing and Computer-Assisted Intervention, Lecture Notes in Computer Science, vol. 1496, Springer, Berlin, 1998, pp. 1153–1161.
[23] A. Rangarajan, H. Chui, E. Mjolsness, S. Pappu, L. Davachi, P. Goldman-Rakic, J. Duncan, A robust point-matching algorithm for autoradiograph alignment, Med. Image Anal. 1 (4) (1997) 379–398.
[24] A. Roche, G. Malandain, X. Pennec, N. Ayache, The correlation ratio as a new similarity measure for multimodal image registration, in: W.M. Wells, A. Colchester, S. Delp (Eds.), Proceedings MICCAI'98, Lecture Notes in Computer Science, vol. 1496, Springer, Berlin, 1998, pp. 1099–1106 (electronic version: http://www.inria.fr/RRRT/RR-3378.html).
[25] P.J. Rousseuw, A.M. Leroy, Robust Regression and Outlier Detection, Wiley Series in Probability and Mathematical Statistics, 1st ed. 1987.
[26] M. Rydmark, T. Jansson, C.-H. Berthold, T. Gustavsson, Computer assisted realignment of light micrograph images from consecutive sections series of cat cerebral cortex, J. Microsc. 165 (1992) 29–47.
[27] T. Schormann, A. Dabringhaus, K. Zilles, Statistics of deformations in histology and application to improved alignment with MRI, IEEE Trans. Med. Imag. 14 (1) (1995) 25–35.
[28] T. Shormann, K. Zilles, Limitation of the principal-axes theory, IEEE Trans. Med. Imag. 16 (6) (1997) 942–947.
[29] A.W. Toga, E.M. Santori, R. Hazani, K. Ambach, A 3D digital map of rat brain, Brain Res. Bull. 38 (1) (1995) pp. 77–85 (data available at: http://www.loni.ucla.edu/data/rat/).
[30] W. Vanduffel, R. Vogels, R.B.H. Tootell, G.A. Orban, Scrambling images of natural objects: II. A double-label deoxyglucose study, Invest. Ophthalmol. Vis. Sci. 38 (S1001) (1997).
[31] B.C. Vemuri, et al., An efficient motion estimator with application to medical image registration, Med. Image Anal. 2 (1) (1998) 79–98.
[32] P. Viola, Alignment by maximisation of mutual information, Int. J. Comput. Vis. 24 (2) (1997) 137–154.
[33] Z. Zhang, Parameter estimation techniques: a tutorial with application to conic fitting, Image Vis. Comput. J. 15 (1) (1997) 59–76.
[34] W. Zhao, T.Y. Young, M.D. Ginsberg, Registration and three-dimensional reconstruction of autoradiographic images by the disparity analysis method, IEEE Trans. Med. Imag. 12 (4) (1993) 782–791.